# Discovery of planetary nebulae in NGC 4214 using SITELLE

Sebastien Vicens-Mouret[a], Laurent Drissen[a], and Carmelle Robert[a]

[a]Département de physique, de génie physique et d'optique, Université Laval, and Centre de recherche en astrophysique du Québec, Québec, Canada

## ABSTRACT

We present data taken with the imaging Fourier transform spectrograph SITELLE, at the Canada-France-Hawaii Telescope, of the nearby dwarf starburst galaxy NGC 4214. From these data, we identify 18 new planetary nebula candidates in the outer part of the galaxy. For each planetary nebula, we provide the flux of the strong emission lines, the [OIII]$\lambda\lambda$5007,4959 H$\alpha$ and H$\beta$, as well as the radial velocity. We also provide the kinematics for 13 of the 17 planetary nebulae previously discovered in the central part of the galaxy with HST data by Dopita et al. (2010). We present a novative technique to obtain accurate velocity measurement for objects with [OIII] emission but without H$\alpha$ emission with SITELLE. We use the [OIII] emission line luminosity function of the planetary nebulae to establish a new velocity-independent distance for the galaxy. This method gives a distance $D = 3.31^{+0.20}_{-0.27}$ Mpc for NGC 4214.

**Keywords:** extra galactic distance, emission line, galaxies, iFTS, luminosity function, NGC 4214, planetary nebula

## 1. INTRODUCTION

SITELLE is the Canada-France-Hawaii Telescope (CFHT) imaging Fourier transform spectrometer that provides millions of spectra ($2024 \times 2048$ pixels) with a resolution R between 1 and 10 000 in a large $11' \times 11'$ field of view with a theoretical spatial sampling of $0.32''$ per pixel (1). SITELLE can cover the entire surface of nearby galaxies while observing several emission lines from 365 to 685 nm and therefore measure simultaneously the flux and the kinematics of the ionized gas related to HII regions, supernova remanants, planetary nebulae, AGNs... All these objects are key elements to understand star formation and the evolution of galaxies. SITELLE inspired the CFHT Large Program SIGNALS (the Star formation, Ionized Gas, and Nebular Abundances Legacy Survey; 2) that is specifically designed to study star formation processes in about 40 nearby galaxies with a spatial resolution between 2 and 40 pc, something never done before! More than 50 000 HII regions will be observed, a highly significant statistical sample of objects in various galactic environments.

NGC 4214 has been observed with SITELLE as part of SIGNALS. This galaxy is a close-by starbust irregular galaxy at a distance of approximately 2.5-3.5 Mpc (3; 4) with a central low metallicity 12+log(O/H) $\simeq$ 8.2 (3; 4; 5; 6). Most studies have focused on either modeling its interstellar medium (ISM) properties (7; 8), its HII regions (9), its young stellar populations (6; 10; 11; 12; 13), or its dust properties (12; 13; 14). NGC 4214 has experienced several episodes of intense star formation, the most recent ones being concentrated in its center and along its bar. Its center contain several hundreds of HII regions. Its dust component is closely coupled with the ionized gas. NGC 4214 shows several extinction free regions as the gas (and the dust) has been blown away by previous star formation events leading to high energy photon leakage.

Planetary nebulae (PNe) are defined as the envelope of gas surrounding a white dwarf. It is the final product of the life of low-mass stars ($M \leq 8\ M_\odot$). As low mass stars live for several billions of years, the study of PNe allows to investigate past episodes of star formation. Indeed, since the chemical envelope of low-mass stars does not change intensively during their lifetime, the chemical composition of PNe reflect the metallicity of the gas at the time of the formation of its progenitor, which gives information on the evolution of the galaxy. Furthermore, because white dwarfs can only cover a limited mass range, it implies that there is an upper limit to the luminosity of a PN; this limit can be used to determine extra-galactic distances. In addition, the study of PNe can provide an easy insight into motion within their galaxy (because the bright [OIII] emission line of PNe can be seen at

Table 1. Observations of NGC 4214 with SITELLE

| Filter | seeing | R | Exposure/step | Num. Steps | Date |
|---|---|---|---|---|---|
| SN2 | 0.76" | 940 | 50s | 219 | June 14, 2018 |
| SN3 | 0.83" | 1900 | 30s | 337 | June 19, 2018 |

large distances), and therefore help measuring the mass of galaxies.

An intensive study of the PNe in NGC 4214 has been done using HST narrow band images (3). It was used to reveal the distance of NGC 4214. This study, however, is limited to the central region of the galaxy due to the small spatial coverage of the HST data and does not recover any kinematic.

Here, we present a new sample of PNe in NGC 4214 based on the study of the strong emission lines available in the SITELLE filters. Two papers are in preparation (Vicens-Mouret et al.) to present more details on NGC 4214 PNe and supernova remnants, and to study the HII regions and the diffuse ionized gas (DIG) of NGC 4214. Section 2 presents the data and their calibrations. Section 3 explains how the identification of the PNe was done. The determination of the distance of NGC 4214, based on the PNe, is presented in Section 4. Section 5 summarizes this work.

## 2. OBSERVATIONS, DATA REDUCTION AND CALIBRATIONS

### 2.1 Observations and data reduction

As part of the SIGNALS galaxy sample, NGC 4214 was observed with the three SITELLE filters: SN1 (363-368 nm) with the emission doublet [OII]$\lambda\lambda$3726,3728, SN2 (482-513 nm) with the emission lines [OIII]$\lambda\lambda$5007,4959 and H$\beta$, and SN3 (647-685 nm) with [NII]$\lambda\lambda$6548,6583, H$\alpha$, and [SII]$\lambda\lambda$6716,6731. As PNe show little to no emission in [OII], the SN1 cube is not mentioned furthermore here. Table 1 summarizes the observing parameters for each filter: the seeing, the spectral resolution R, the observing time (given by the product of the number of steps and exposure time per step) and the date of observation. The resolution of the SN3 cube is higher as it will be useful to disentangle the [NII] doublet from H$\alpha$ and to properly study the emission gas velocity and the emission gas velocity dispersion. Figure 1 shows the SITELLE's image of NGC 4214. This image was created by combining the SN2 and SN3 deepframes (i.e. the sum of all the interferograms for a datacube).

The datacubes have been reduced using ORBS (15), SITELLE's dedicated data reduction software. ORBS converts the raw interferograms by Fourier transform in datacubes in units of wavenumber ($cm^{-1}$). It takes into account biases and flats. A standard star (GD71) was used for the flux calibration and a 543.5 nm laser was observed with the telescope at the zenith for the calibration in wavenumber.

As the datacubes have been observed at different epochs, they can suffer from misalignment. Using several bright foregrounds stars in the field, we find a negligible shift (below 1 pixel) between SN2 and SN3. Considering the small change in seeing measured for the two datacube (see Tab. 1), no spatial degradation has been done to match their resolutions.

We use SITELLE's software ORCS to measure the emission lines (15). For each pixel within a filter, the emission lines are simultaneously modeled with a sincgauss function, i.e. the convolution of a Gaussian with the instrument sinc profile (16). ORCS returns the line flux, amplitude, continuum level, radial velocity, and the line broadening (the velocity dispersion), as well as the respective uncertainties.

Once the observed flux are measured, they are corrected for the foreground extinction using Pyneb (17), assuming the extinction law for the Milky Way (18), with $A_V = 0.06$ (from NED) and $R_V = 3.1$. While the intrinsic extinction (from the dust inside the galaxy) is an important correction to make (the corrected flux can be up to $10 times$ bigger than observed), it has been shown however that in NGC 4214, the dust is coupled to the gas (6). As the vast majority of our PNe lies in the outer part of the galaxy, where there are very little to no gas around, no intrinsic correction has been done. It is nonetheless a caveat for the few PNe in the center of the galaxy.

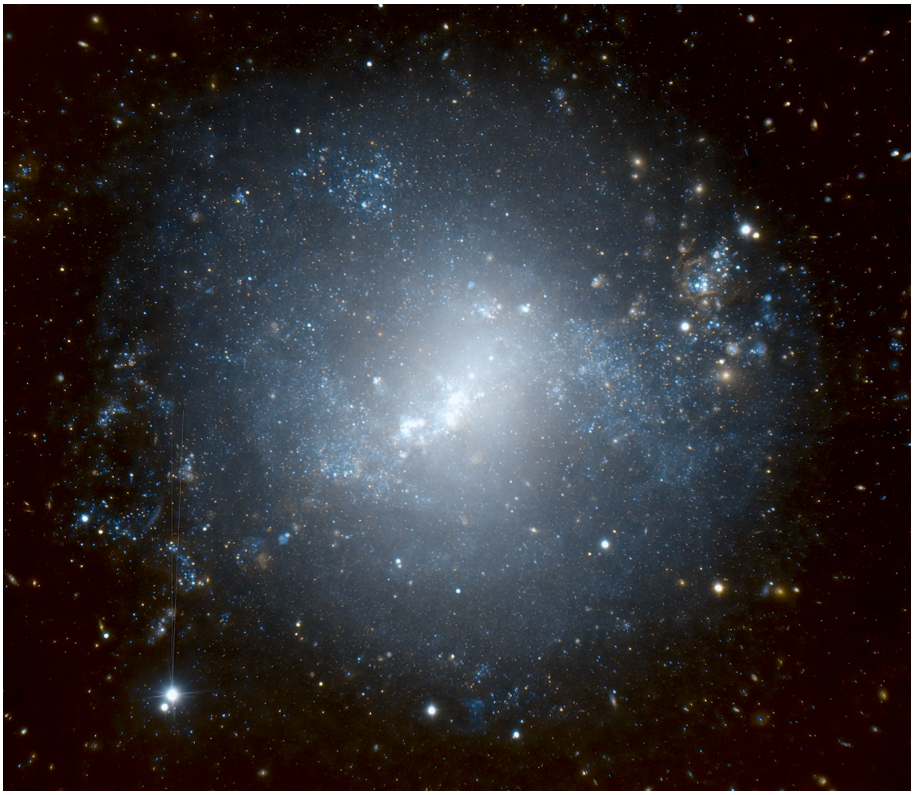

Figure 1. SITELLE's image of NGC 4214 combining the SN3 deepframe (in red) with the SN2 deepframe (in blue) and the mean of both (in green).

## 2.2 Calibration

### 2.2.1 Aperture Photometry and Flux Calibration

As PNe are unresolved faint objects in extra-galactic studies, we measure their flux in a 3 pixels radius aperture and multiply it by an aperture correction factor to extract their total flux. This methodology ensure a higher precision for very faint objects for which it is often hard to delimit the boundaries. To determine the correction factor, we studied the cumulative flux in expending rings around 12 foreground stars. On average, the 3 pixels aperture corresponds to 82.7 % for the SN2 filter, and 84.2 % for the SN3 filter.

For all our observed objects, we correct for the sky emission line, the local emission (i.e. from the diffuse surrounding gas), and the local absorption features (from the underlying galaxy stellar populations), by subtracting a local background spectrum. To create the background spectrum, we retain only pixels in a circular aperture around the PN, with lower [OIII] emission than for the brightest PN pixel. We require that the total number of pixels in the background be at least equal to the number of pixels selected for the source.

As a proof of the validity of our flux calibration and our aperture correction factor, we measured the flux in SITELLE data for several PNe that are in the previously published catalog for NGC 4214 using HST data, i.e. several narrow band images centered on [OIII], H$\alpha$ and H$\beta$ (3). The [OIII]$\lambda$5007 line flux comparison is shown in Figure 2. We globally find a good agreement for most PNe, except D4, D8, and D14. While D8 is embedded in diffuse emission gas, D4 and D14 are objects with very little background emission and are close to the 20% confidence level. Since the spatial resolution of SITELLE is lower than for the HST data, some deviation is not suprizing as it is difficult to consider the same background correction.

### 2.2.2 Velocity calibration

From the emission line positions, we retrieve the velocity of the ionized gas. The datacubes are calibrated in wavenumber (i.e. velocity) using the laser, but because there are changes in the conditions (temperature,

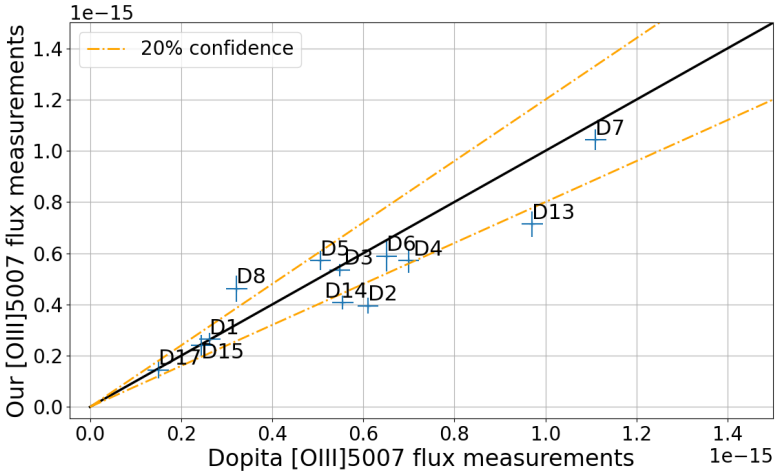


Figure 2. Comparison of PNe [OIII]$\lambda$ 5007 flux measurements with those of (3). We find a very good agreement for most sources, except D8, D4 and D14 as explained in the text, suggesting a 20 % confidence levels for our flux measurements.

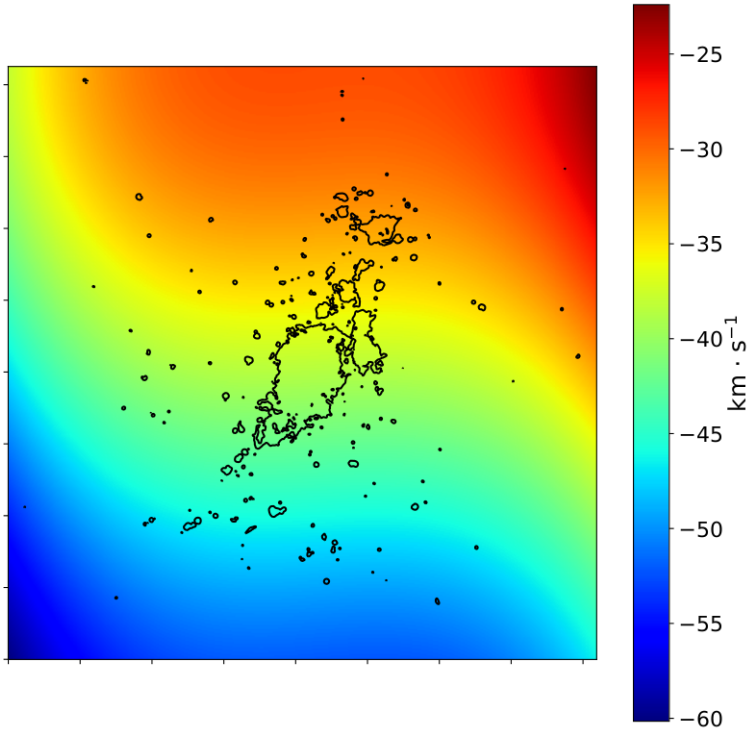


Figure 3. Velocity map of the SN3 OH emission lines on the line of sight of NGC 4214. The black contour shows the galaxy H$\alpha$ emission flux at $5 \times 10^{-17}$ erg s$^{-1}$ cm$^{-2}$ Å$^{-1}$. The OH sky line velocity varies smoothly with a small spread less than 20 km s$^{-1}$ over the galaxy.

telescope orientation) between the laser and the galaxy observation, the velocity measurements may not be absolute. In the case of the SN3 filters, we can correct this effect by using a set of strong sky OH emission lines present in this filter. ORCS was used to map the SN3 OH sky lines, reveling a small systematic velocity shift less than 20 km s$^{-1}$ from the North to the South side of the galaxy (see Fig. 3). Correcting this shift allow us to measure the SN3 absolute velocity with a precision of 1-2 km s$^{-1}$ (19).

For several PNe, we see little to no H$\alpha$ emission, preventing us to obtain an absolute velocity measurement

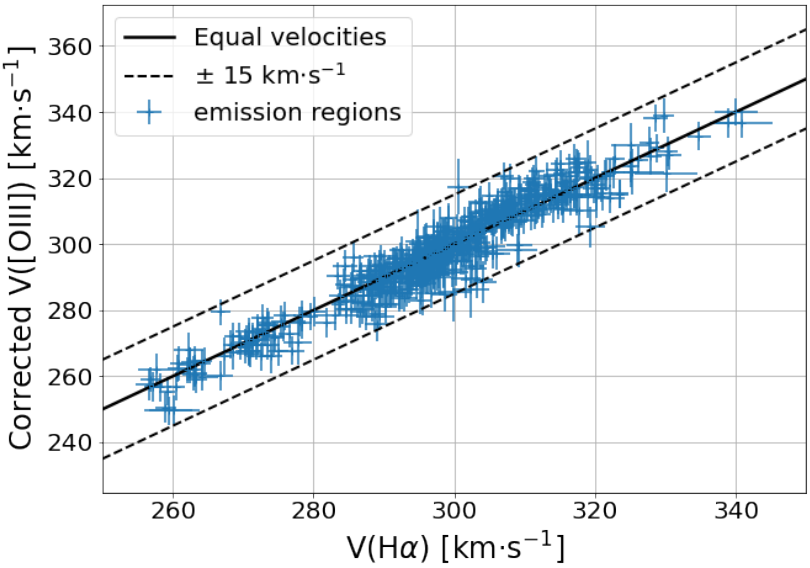


Figure 4. Comparison of the velocity obtained with our calibration between the SN2 and SN3 filters for the HII regions used for the calibration. All refined velocity lie below the 15 km s$^{-1}$ level confidence.

with the SN3 data, but we observe a very clear [OIII] emission in the SN2 data that can be used to determine a velocity. However, there are no strong OH sky emission lines in the SN2 datacube and a different method must be considered here to get an absolute velocity from the [OIII] line. This method simply implies to compare the SN3-H$\alpha$ absolute and SN2-[OIII] relative velocities for bright HII regions located near the PNe (see Vicens-Mouret et al. in prep for more details about the detection of the HII regions). The calibrated PNe velocity is given as:

$$V_{\rm calibrated} = V_{\rm [OIII]} + \Delta V, \tag{1}$$

$$\Delta V = \frac{\sum_i^{N_{\rm emit}} V_{\rm emit}(H\alpha) - V_{\rm emit}([OIII])}{N_{\rm emit}}, \tag{2}$$

with $N_{\rm emit}$ being the number of bright emitters within 150 pixels of the studied PN, $V_{\rm emit}(H\alpha)$ and $V_{\rm HII}([OIII])$ are the velocity measured in H$\alpha$ and [OIII] respectively, for the emission line regions. Figure 4 highlights the effectiveness of our calibration. For the full bright emission line region sample, we are able to retrieve the velocity measured in the SN3 filter using the calibrated SN2 velocity with a confidence of 15 km s$^{-1}$. This method allow us to measure accurate velocities for 7 PNe for which there is no H$\alpha$ emission and to improve the velocity measurement for 5 other PNe.

## 3. PLANETARY NEBULAE IDENTIFICATION

PN candidates are first visually identified as bright unresolved [OIII] sources (as in 20). As a second step, we look at their [OIII]$\lambda$5007/H$\beta$ ratio and only retain objects with [OIII]$\lambda$5007/H$\beta \geq 3$ (following 21). Figures 5 and 6 show the [OIII] and H$\alpha$ image and the spectrum near these lines for two PNe as examples, one is in the central part of the galaxy (D7) and one in the outer part (VD1).

We find 18 new PNe in the outer part of NGC 4214 with SITELLE data. In addition, we find 13 out of the 17 PNe listed in the previous HST catalog (3); the 4 remaining HST PNe are deeply embedded in DIG emission and we are unable to detect them. Among the detected ones, two sources show [OIII]$\lambda$5007/H$\beta$ between 2.5 and

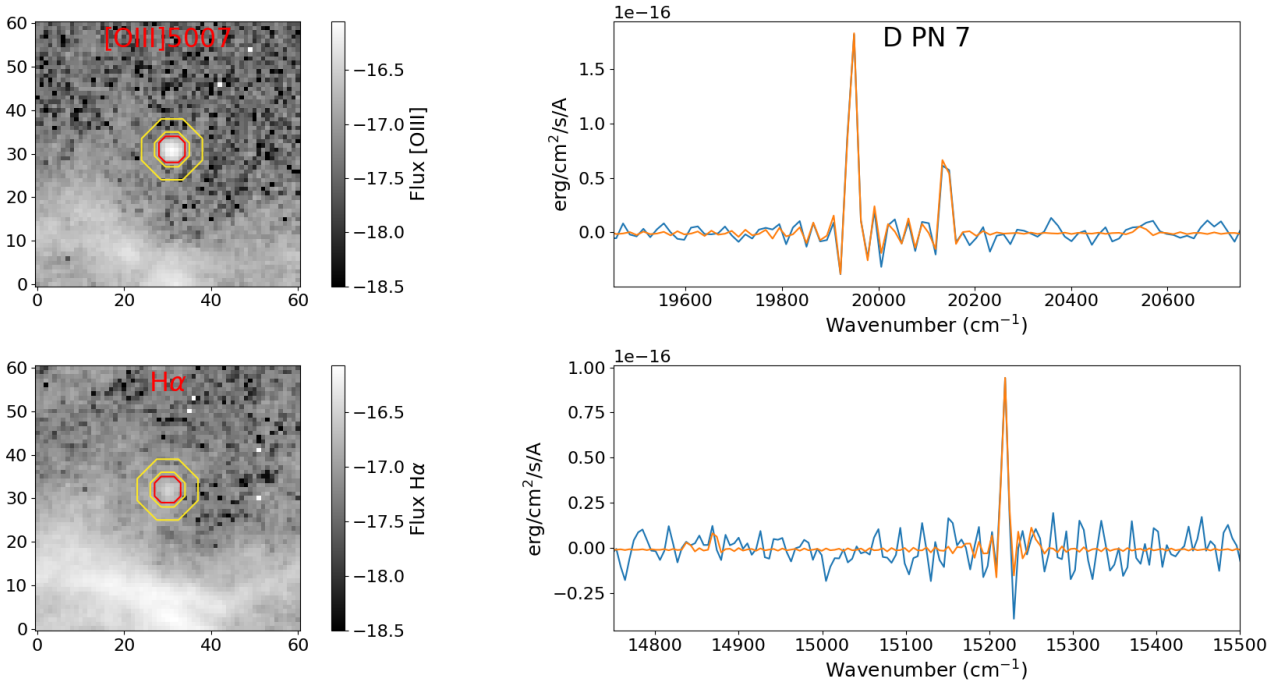


Figure 5. [OIII]5007 emission, SN2 filter spectrum in the top panel as well as H$\alpha$ emission and SN3 filter spectrum in the lower panel of the PN D7.

3: 1) VD7 has a ratio of 2.7 but if we take into account the 40% uncertainty of its H$\beta$ line, it could lie above the limit; and 2) D13 has a ratio of 2.6, but since it is very sensitive to our background spectrum and since the HST ratio is 3.8 (3), we kept it in our sample. This lead to a total of 31 PNe discovered with SITELLE in NGC 4214.

## 4. THE DISTANCE OF NGC 4214 BASED ON ITS PNE

It has been shown (22) that the planetary nebula luminosity function (PNLF) follows empirically an equation of the form:

$$N(M) \propto e^{0.307\,M} \cdot \left(1 - e^{3(M^* - M)}\right), \tag{3}$$

where $M$ is the absolute magnitude and $M^*$ is the absolute magnitude of the most luminous PN that could possibly exist (22; 23). It is proposed (24) that the $M^*$ bright cutoff is mostly constant for Z $<$ 8.45. We adopt $M^* = -4.20^{+0.11}_{-0.17}$ mag as determined for the Small Magellanic Cloud (25) since the metallicity of NGC 4214 lies between the Small and Large Magellanic cloud metallicity (3; 5; 6). The bright cutoff, when observed at a given apparent magnitude, can be used to constraint the distance to the galaxy.

Several methods exist to determine the distance of a galaxy using the PNLF. One can use the brightest PN is its sample and assume it stand on the cutoff. This method, although approximate, can yield a good result specially for big sample. It was used with the HST PNe sample of NGC 4214 (3) and a distance D = 3.19±0.36 Mpc was obtained. Another simple method consists to bin in magnitude the PNe sample and to fit the data with the PNLF equation. While this method is much more precise than the previous one, it is still biased by the bins width and the number of objects. Here we use the maximum likelihood method (22) which removes any bias introduced by the magnitude bin width and is particularly well suited for our small sample. The PNLF can be seen as a probabilistic distribution depending solely on the distance. Each PN in the sample can then be seen in term of a probability. We can compute a likelihood as the product of all the probabilities. The distance with the highest likelihood is then the most probable distance.

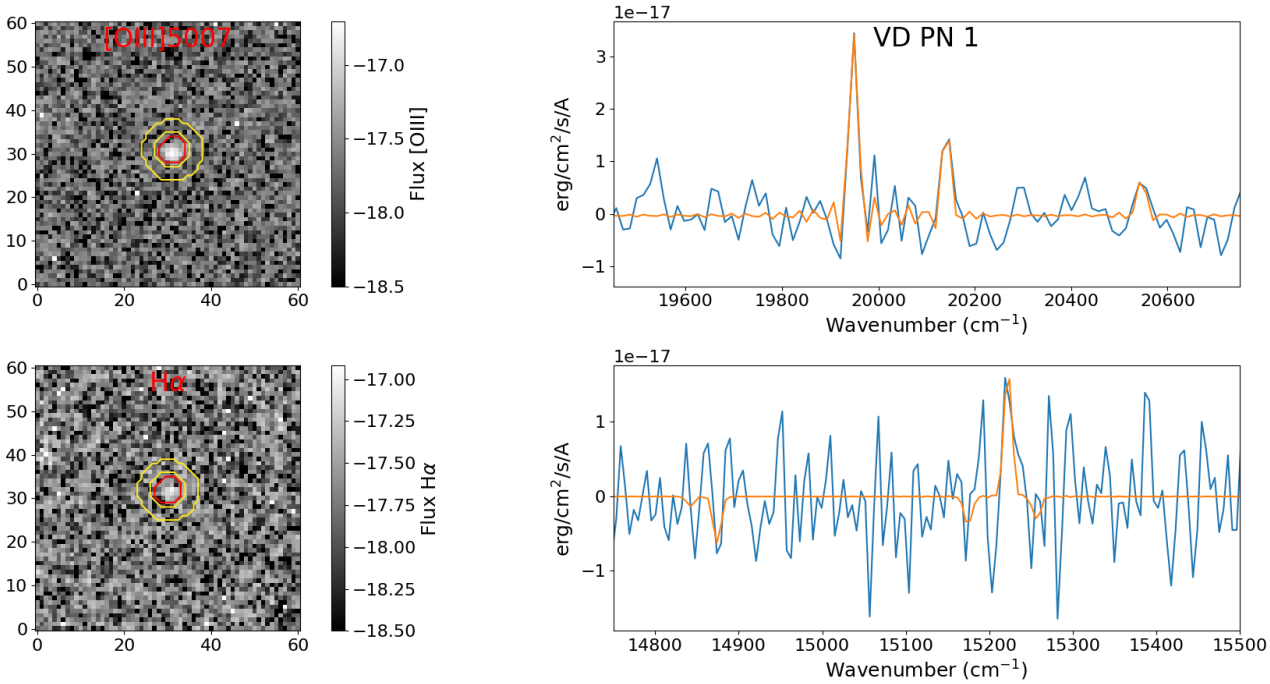


Figure 6. [OIII]5007 emission, SN2 filter spectrum in the top panel as well as H$\alpha$ emission and SN3 filter spectrum in the lower panel of the PN VD1.

However one problem may arise if we use the full PNe sample. While faint PNe have a higher probability to be observed, it is however very likely that we miss to detect a lot of these objects. In order to avoid some bias due to missing objects at a given magnitude, we estimated first our completeness threshold. To determine our completeness threshold, we created mock PNe with low magnitudes (we only simulate the [OIII] emission), injected them into the data, and tried to recover them. For each half magnitude from 23 and 27, we randomly injected 5 times 20 PNe over the [OIII] galaxy map. We found that for magnitudes below 26, we always recover more than 80% of the injected mocks. We never recover 100% because as we randomly distribute them, mock PNe can sometime overlap with HII regions. We finally set our completeness threshold to 26 mag. 24 PNe remain in our sample to determine the distance.

We also want to propagate the flux uncertainties into the distance uncertainty. Therefore, we built for each PN a magnitude distribution with the shape of a Gaussian centered on the PN magnitude with its broadening $\sigma$ equal to the PN magnitude uncertainty. We then produced 7800 combinations out of 24 PNe (each giving a distance modulus using the maximum likelihood method). In each combination, the magnitude of the PN is randomly chosen following the previously defined distribution. Our method gives the distance modulus posterior distribution shown in Figure 7. Propagating the uncertainty for $M^*$, it leads finally to a distance modulus $\mu = 27.60^{+0.13}_{-0.19}$ mag, i.e. to a distance $D = 3.31^{+0.20}_{-0.27}$ Mpc for NGC 4214. This is very close to the HST PNe distance of 3.19±0.36 Mpc (3). It is good to remember that neither the HST study or us corrected the PNe in the central part of the galaxy for the intrinsic extinction. Correcting for extinction would increase the brightest PNe magnitude and would then lead to a smaller distance.

## 5. CONCLUSION

Using SITELLE data, we discover 18 new PN in the outer part of NGC 4214. PNe are visually detected as unresolved objects in the [OIII] map and are latter confirmed by studying their [OIII]/H$\beta$ ratio. For each PN, we provide [OIII] magnitude and flux, H$\beta$ flux, H$\alpha$ flux and a radial velocity, either directly measured using

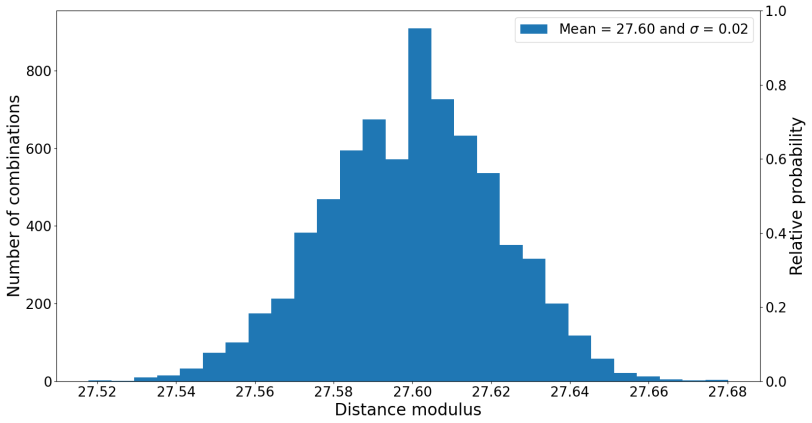


Figure 7. Distance modulus distribution from 7800 combinations of the 24 PNe in our sample after setting a completeness threshold. For every combination, the magnitude of each PN is randomly chosen following a Gaussian distribution centred on the observed magnitude with its broadening$\sigma$ equal to the magnitude uncertainty of the observation. We find that the most probable distance modulus for NGC 4214 is $\mu = 27.60 \pm 0.02$ mag (D = $3.31^{+0.20}_{-0.27}$ Mpc) for $M^* = -4.20^{+0.11}_{-0.17}$ mag.

the H$\alpha$ line or by calibrating the [OIII] velocity using nearby HII regions. We provide as well this information for the 13 of the 17 PNe found from HST data (3) in the central part of NGC 4214. With this more complete SITELLE sample of 31 PNe, we combined the maximum likelihood method with the PNLF method (22) to derive a distance for NGC 4214 of $3.31^{+0.20}_{-0.27}$ Mpc. The uncertainty of our measurement take into account the flux uncertainty as well as the $M^*$ uncertainty of the PNLF relation. We find a very good agreement with the previous HST measurement (3).


## Acknowledgements

This work is based on observations obtained with SITELLE, a joint project of Université Laval, ABB, Université de Montréal, and the Canada-France-Hawaii Telescope which is operated by the National Research Council of Canada, the Institut National des Sciences de l'Univers of the Centre National de la Recherche Scientifique of France, and the University of Hawaii. The authors wish to recognize and acknowledge the very significant cultural role that the summit of Mauna Kea has always had within the indigenous Hawaiian community. We are most grateful to have the opportunity to conduct observations from this mountain. LD and CR are grateful to the Natural Sciences and Engineering Research Council of Canada and the Fonds de Recherche du Québec: Nature et technologies. This research made use of Astropy, a community-developed core Python package for Astronomy, and has made use of NASAs Astrophysics Data System Bibliographic Services.


## ACKNOWLEDGMENTS

## References


[1] Drissen, L., Martin, T., Rousseau-Nepton, L., Robert, C., Martin, R. P., Baril, M., Prunet, S., Joncas, G., Thibault, S., Brousseau, D., Mandar, J., Grandmont, F., Yee, H., and Simard, L., "SITELLE: an Imaging Fourier Transform Spectrometer for the Canada-France-Hawaii Telescope," **485**, 3930–3946 (May 2019).

[2] Rousseau-Nepton, L., Martin, R. P., Robert, C., Drissen, L., Amram, P., Prunet, S., Martin, T., Moumen, I., Adamo, A., Alarie, A., Barmby, P., Boselli, A., Bresolin, F., Bureau, M., Chemin, L., Fernandes, R. C., Combes, F., Crowder, C., Della Bruna, L., Duarte Puertas, S., Egusa, F., Epinat, B., Ksoll, V. F., Girard, M., Gómez Llanos, V., Gouliermis, D., Grasha, K., Higgs, C., Hlavacek-Larrondo, J., Ho, I. T., Iglesias-Páramo, J., Joncas, G., Kam, Z. S., Karera, P., Kennicutt, R. C., Klessen, R. S., Lianou, S., Liu, L., Liu, Q., de Amorim, A. L., Lyman, J. D., Martel, H., Mazzilli-Ciraulo, B., McLeod, A. F., Melchior, A. L., Millan, I., Mollá, M., Momose, R., Morisset, C., Pan, H. A., Pati, A. K., Pellerin, A., Pellegrini, E., Pérez, I., Petric,

A., Plana, H., Rahner, D., Ruiz Lara, T., Sánchez-Menguiano, L., Spekkens, K., Stasińska, G., Takamiya, M., Vale Asari, N., and Vílchez, J. M., "SIGNALS: I. Survey description," **489**, 5530–5546 (Nov. 2019).

[3] Dopita, M. A., Calzetti, D., Maíz Apellániz, J., Blair, W. P., Long, K. S., Mutchler, M., Whitmore, B. C., Bond, H. E., MacKenty, J., Balick, B., Carollo, M., Disney, M., Frogel, J. A., O'Connell, R., Hall, D., Holtzman, J. A., Kimble, R. A., McCarthy, P., Paresce, F., Saha, A., Walker, A. R., Silk, J., Sirianni, M., Trauger, J., Windhorst, R., and Young, E., "Supernova remnants, planetary nebulae and the distance to NGC 4214," **330**, 123–131 (Nov. 2010).

[4] Maíz-Apellániz, J., Cieza, L., and MacKenty, J. W., "Tip of the red giant branch distances to NGC 4214, UGC 685, and UGC 5456," *The Astronomical Journal* **123**, 1307–1315 (mar 2002).

[5] Pilyugin, L. S., Grebel, E. K., and Zinchenko, I. A., "On the radial abundance gradients in discs of irregular galaxies," **450**, 3254–3263 (July 2015).

[6] MacKenty, J. W., Maíz-Apellániz, J., Pickens, C. E., Norman, C. A., and Walborn, N. R., "Hubble space telescope/WFPC2 and VLA observations of the ionized gas in the dwarf starburst galaxy NGC 4214," **120**, 3007–3026. ADS Bibcode: 2000AJ....120.3007M.

[7] Dimaratos, A., Cormier, D., Bigiel, F., and Madden, S. C., "Modeling the physical properties in the ISM of the low-metallicity galaxy NGC 4214," **580**, A135 (Aug. 2015).

[8] Fahrion, K., Cormier, D., Bigiel, F., Hony, S., Abel, N. P., Cigan, P., Csengeri, T., Graf, U. U., Lebouteiller, V., Madden, S. C., Wu, R., and Young, L., "Disentangling the ISM phases of the dwarf galaxy NGC 4214 using [C II] SOFIA/GREAT observations," **599**, A9 (Mar. 2017).

[9] Hartmann, L. W., Geller, M. J., and Huchra, J. P., "Kinematics of H II regions in the blue irregulars NGC 4214 and NGC 4449.," **92**, 1278–1290 (Dec. 1986).

[10] McQuinn, K. B. W., Skillman, E. D., Cannon, J. M., Dalcanton, J., Dolphin, A., Hidalgo-Rodríguez, S., Holtzman, J., Stark, D., Weisz, D., and Williams, B., "The Nature of Starbursts. II. The Duration of Starbursts in Dwarf Galaxies," **724**, 49–58 (Nov. 2010).

[11] Andrews, J. E., Calzetti, D., Chandar, R., Lee, J. C., Elmegreen, B. G., Kennicutt, R. C., Whitmore, B., Kissel, J. S., da Silva, R. L., Krumholz, M. R., O'Connell, R. W., Dopita, M. A., Frogel, J. A., and Kim, H., "An Initial Mass Function Study of the Dwarf Starburst Galaxy NGC 4214," **767**, 51 (Apr. 2013).

[12] Úbeda, L., Maíz-Apellániz, J., and MacKenty, J. W., "The young stellar population of NGC 4214 as observed with the hubble space telescope. i. data and methods," **133**, 917–931. ADS Bibcode: 2007AJ....133..917U.

[13] Úbeda, L., Maíz-Apellániz, J., and MacKenty, J. W., "The young stellar population of NGC 4214 as observed with the hubble space telescope. II. results," **133**, 932–951. ADS Bibcode: 2007AJ....133..932U.

[14] Hermelo, I., Lisenfeld, U., Relaño, M., Tuffs, R. J., Popescu, C. C., and Groves, B., "The dust SED of dwarf galaxies. i. the case of NGC 4214," **549**, A70.

[15] Martin, T., Drissen, L., and Joncas, G., "ORBS, ORCS, OACS, a Software Suite for Data Reduction and Analysis of the Hyperspectral Imagers SITELLE and SpIOMM," in [*Astronomical Data Analysis Software an Systems XXIV (ADASS XXIV)*], Taylor, A. R. and Rosolowsky, E., eds., *Astronomical Society of the Pacific Conference Series* **495**, 327 (Sept. 2015).

[16] Martin, T. B., Prunet, S., and Drissen, L., "Optimal fitting of Gaussian-apodized or under-resolved emission lines in Fourier transform spectra providing new insights on the velocity structure of NGC 6720," **463**, 4223–4238 (Dec. 2016).

[17] Luridiana, V., Morisset, C., and Shaw, R. A., "PyNeb: a new tool for analyzing emission lines. I. Code description and validation of results," **573**, A42 (Jan. 2015).

[18] Fitzpatrick, E. L., "Correcting for the Effects of Interstellar Extinction," **111**, 63–75 (Jan. 1999).

[19] Martin, T. B., Drissen, L., and Melchior, A.-L., "A SITELLE view of M31's central region - I. Calibrations and radial velocity catalogue of nearly 800 emission-line point-like sources," **473**, 4130–4149 (Jan. 2018).

[20] Roth, M. M., Jacoby, G. H., Ciardullo, R., Davis, B. D., Chase, O., and Weilbacher, P. M., "Toward Precision Cosmology with Improved PNLF Distances Using VLT-MUSEI. Methodology and Tests," **916**, 21 (July 2021).

[21] Delgado-Inglada, G., García-Rojas, J., Stasińska, G., and Rechy-García, J. S., "A study of extragalactic planetary nebulae populations based on spectroscopy. I. Data compilation and first findings," **498**, 5367–5385 (Nov. 2020).

[22] Ciardullo, R., Jacoby, G. H., Ford, H. C., and Neill, J. D., "Planetary Nebulae as Standard Candles. II. The Calibration in M31 and Its Companions," **339**, 53 (Apr. 1989).

[23] Jacoby, G. H., Branch, D., Ciardullo, R., Davies, R. L., Harris, W. E., Pierce, M. J., Pritchet, C. J., Tonry, J. L., and Welch, D. L., "A Critical Review of Selected Techniques for Measuring Extragalactic Distances," **104**, 599 (Aug. 1992).

[24] Ciardullo, R., "The Planetary Nebula Luminosity Function at the dawn of Gaia," **341**, 151–161 (Sept. 2012).

[25] Ciardullo, R. and Jacoby, G. H., "Planetary Nebulae as Standard Candles. VIII. Evidence for a Change in the Luminosity Function Cutoff at Low Metallicity," **388**, 268 (Apr. 1992).